ACS APPLIED MATERIALS & INTERFACES

Research Article

www.acsami.org

Three-Dimensional Hierarchically Porous All-Carbon Foams for Supercapacitor

Bo You,*[,†] Jinhui Jiang,[†] and Sanjun Fan[‡]

[†]Department of Chemistry, University of Science and Technology of China, Hefei, Anhui 230026, China

[‡]Department of Chemistry and Biochemistry, Auburn University, Auburn, Alabama 36849-5312, United States

Supporting Information

ABSTRACT: Three-dimensional hierarchically porous carbon-CNT-graphene ternary all-carbon foams (3D-HPCFs) with 3D macro- and mesoporous structures, a high specific surface area (1286 m^2 g^{-1}), large bimodal mesopores (5.1 and 2.7 nm), and excellent conductivity have been fabricated through multicomponent surface self-assembly of graphene oxide (GO)-dispersed pristine CNTs (GOCs) supported on a commercial sponge. The commercial sponge with a 3D interconnected macroporous framework not only is used as a support for GOCs and subsequently multicomponent self-assembly but also serves as a 3D scaffold to buffer electrolytes to reduce ion transport resistance and ion diffusion distance, while the GO acts as "surfactant" to directly disperse pristine CNTs, preserving the excellent electronic structure of pristine CNTs, and the CNTs also prevent the aggregation of graphene as well as improve the whole conductivity. Benefiting from the aforementioned characteristics, the 3D-HPCFs-based supercapacitors show outstanding specific capacitance, high rate capability, and excellent cycling stability, making them potentially promising for high-performance energy storage devices.

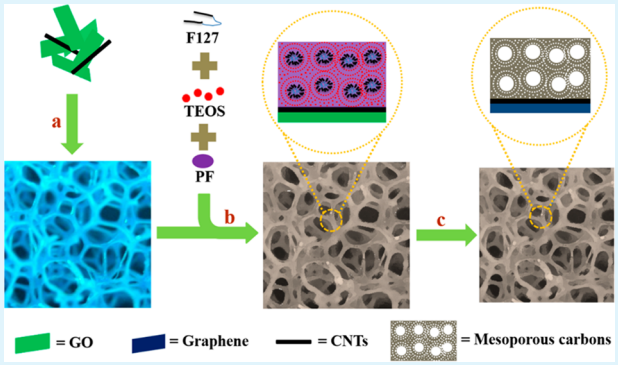

KEYWORDS: *graphene, CNTs, porous, supercapacitor*

INTRODUCTION

The critical issue of climate change and rapidly increasing global energy consumption have triggered tremendous research efforts for clean and renewable energy sources.[1,2] With a growing number of requirements for renewable energy production from solar or wind, efficient energy storage devices (ESDs) are needed.[2] As a new class of ESDs, supercapacitors (SCs) with high power density, excellent cycling stability, and superior performance in extreme temperatures are now attracting intensive attention for many portable systems and hybrid electric vehicles.[3−8] Porous carbon materials, especially the activated carbons, remain the most common and important electrode candidates for SCs due to their stable physicochemical properties, low-cost, and availability.[9−11] However, the activated carbon-based SCs usually suffer from electrode kinetic problems and mediocre conductivity due to the small pore size (which impedes the effective ion transport) and amorphous structure, respectively.[12] Therefore, considerable efforts have been focusing on increasing the specific capacitance of porous carbon-based SCs by tailoring their specific surface area and pore size distribution (PSD) as well as conductivity.[13]

Three-dimensional (3D) hierarchically porous carbons are strongly recommended for SCs.[12,14] For these porous materials, the macropores and mesopores with 3D configurations can buffer electrolytes to reduce ion transport resistance and ion diffusion distance for high-rate SCs applications, and the large accessible specific surface area of mesopores can also enhance the charge storage. On the other hand, introducing nanocarbon materials with high conductivity (such as graphene and CNTs) can evidently decrease electron transport resistance.[10,15] Ruoff's group used potassium hydroxide to activate microwave exfoliated GO to synthesize 3D porous graphene with a high specific surface area of ∼3100 m^2 g^{-1}.[3,13] Cheng's group used the same activation strategy to fabricate graphene-based porous carbons (GPCs), the specific surface area of the resulting GPCs is high to 3400 m^2 g^{-1}.[13,15] The similar activation (CO_2 activation) strategy was also used to prepare CNT-based porous carbons.[10] Unfortunately, these methods may destroy the conjugated structure of graphene or CNTs and then reduce the conductivity of the composites, and the high fraction of micropores may be incapable of contributing to charge storage.[12] Most recently, Müllen's group have developed a nanocasting approach for synthesis of 3D graphene-based carbon frameworks (3D-GFs) with hierarchical macro- and mesoporous structures.[16] The resulting 3D-GFs exhibit moderate mesopores (2−3.5 nm), low mass density, and excellent conductivity. Nevertheless, except for the time-consuming process of nanocasting and repeated freeze-dying,

Received: June 14, 2014
Accepted: August 13, 2014
Published: August 13, 2014

the 3D-GFs exhibit a low specific surface area (295 m^2 g^{-1}) probably due to the aggregation of reduced graphene oxides. Thus, albeit with great successes regarding 3D hierarchically porous carbons, major challenges still exist, such as the poor solubility of CNTs, the aggregation tendency of CNTs and graphene, and the simultaneous regulation of high surface area and large hierarchical pores.

Herein, we report the rational design and synthesis of new 3D hierarchically porous carbon-CNT-graphene ternary all-carbon foams (3D-HPCFs) through multicomponent surface self-assembly of graphene oxide (GO)-dispersed pristine CNTs (GOCs) supported on the commercial sponge (GOCSs). Specifically, the sponge with an interconnected macroporous framework not only functions as a support for GOCs and subsequently multicomponent self-assembly but also serves as a 3D scaffold, which shortens the ion/electron transport distances. The GO can act as "surfactant" to disperse pristine CNTs directly, preserving the excellent electronic structure of pristine CNTs, and the CNTs also prevent the aggregation of graphene as well as improve the whole conductivity. The large amounts of mesopores with high surface area promote ion transport/charge storage. Benefiting from the aforementioned properties, the 3D-HPCFs-based supercapacitor shows outstanding specific capacitance, high rate capability, and excellent cycling stability, which suggest that such a hybrid architecture is very promising for next-generation high-performance supercapacitors.

EXPERIMENTAL SECTION

Materials. Tetraethyl orthosilicate (TEOS), phenol, formaldehyde solution (37%), NaOH, HCl, HF solution (40%), and ethanol were purchased from Sinopharm Chemical Reagent Co., Ltd. Pluronic F127 (MW = 12 600, $PEO_{106}PPO_{70}PEO_{106}$) was purchased from Sigma-Aldrich Corp.; graphene oxide (GO) was purchased from Nanjing XFNANO Materials TECH Co., Ltd. All chemicals were used as received without any further purification. Doubly distilled water was used in all experiments.

Preparation of GOCs Supported on Sponge (GOCSs). The GO-dispersed pristine CNTs (GOCs) were first prepared according to our method reported previously with little modification.[8] Briefly, 4 mg of GO was added in 5 mL of water with ultrasonication for 1 h. Subsequently, the obtained GO suspensions (0.8 g L^{-1}) were mixed with 1.2 mg of pristine CNTs (30% weight of the GO) and then sonicated for another 1 h; the black colloidal dispersions with no visible precipitation were formed (GOCs, Figure S1, Supporting Information). Second, the commercial macroporous available sponge was cleaned with ethanol and water for several times, followed by completely drying and cutting into small pieces about 2 mm in thickness with a 1 × 1 cm^2 cross section; the as-prepared sponges were dipped into the GOC suspensions and then dried in an oven for 1 h. Such procedures can be repeated to increase the GOC loading in the sponge.

Fabrication of 3D Hierarchically Porous All-Carbon Foams (3D-HPCFs). In a typical preparation, 0.8 g of triblock copolymer F127 was dissolved in 4.0 g of ethanol with 0.5 g of 0.2 M HCl, and the mixture was stirred for 1 h at 40 °C to obtain a clear solution. Next, 1.04 g of TEOS and 2.5 g of 20 wt % phenol–formaldehyde resol (PF) ethanol solution[18] were added in sequence. After 1.5 h of stirring, the resulting GOCSs were dipped into the above mixture and then dried at room temperature to evaporate ethanol before thermopolymerization at 100 °C for 24 h. The dipping, evaporation, and polymerization steps can be repeated to increase the PF loading in the GOCSs. Finally, the as-made specimens were calcined in a tubular furnace at 850 °C for 2 h under Ar, followed by HF etching for the removal of silica, and the 3D-HPCFs were obtained.

Synthesis of the Control Samples. The fabrication of 3D hierarchically mesoporous carbons (3D-HPMCs) and bimodal ordered mesoporous carbon monoliths (OMCs) is similar to that of 3D-HPCFs without involving GOCs and GOCSs, respectively. The graphene-CNTs (GCs) were prepared as follows. Briefly, 8 mg of GO was dissolved in 10 mL of water with ultrasonication for 1 h. Subsequently, the obtained GO suspensions (0.8 g L^{-1}) were mixed with 2.4 mg of pristine CNTs (30% of the GO) and then sonicated for another 1 h. The black colloidal dispersions with no visible precipitation were then freeze-dried and calcined in a tubular furnace at 850 °C for 2 h under Ar, and finally, the GCs were obtained. The FDU-15 ordered mesoporous carbons without complementary mesopores were prepared according to Zhao's group with some modification.[11] In a typical synthesis, 1.0 g of F127 was dissolved in 20 g of ethanol; then, the above PF ethanol solution containing phenol (0.61 g, 6.50 mmol) and (0.39 g, 13.0 mmol) formaldehyde was added by stirring for 10 min to form a homogeneous solution. The solution was transferred to a dish, and the ethanol evaporated at room temperature over 8 h to produce a transparent membrane. The membrane was then heated in an oven at 100 °C for 24 h to thermopolymerize the phenolic resins. The products were calcined at 850 °C for 2 h under Ar to obtain the FDU-15 ordered mesoporous carbons without complementary mesopores.

Characterization. Transmission electron microscopy (TEM) measurements were taken on a JEM 2100F microscope (JEOL, Japan) operated at 200 kV. The samples were crushed into powder and dispersed in ethanol before analysis. Scanning electron microscopy (SEM) measurements were taken on a Sirion 200 microscope (FEI, USA) operated at 5 kV. Nitrogen sorption isotherms were measured at 77 K with a Micromertics ASAP 3020 analyzer (Micromertics, USA). The samples were degassed in a vacuum at 200 °C for at least 5 h before measurements. The Brunauer–Emmett–Teller (BET) method and the Barrett–Joyner–Halenda (BJH) model were utilized to calculate the specific surface area (BET), the pore volumes, and pore size distributions, respectively. The total pore volumes (V_t) were estimated from the adsorbed amount at a relative pressure P/P_0 of 0.994. Thermal gravimetric analysis was monitored using an SDT Q600 analyzer (TA, USA) from room temperature to 850 °C under Ar with a heating rate of 10 °C/min. Raman spectra were obtained with a Labram-HR (Johin-Yvon, France) using a He–Ne laser with an excitation wavelength of 514.5 nm.

Electrochemical Measurement. The electrochemical properties of the as-prepared samples were investigated with a CHI 660A electrochemical workstation (Chenhua, Shanghai) using cyclic voltammetry (CV), galvanostatic charge/discharge (GV), and electrochemical impedance spectroscopy (EIS) techniques in a conventional three-electrode cell. The three-electrode cell configuration consisted of Pt wire as the counter electrode, a saturated calomel electrode (SCE) as the reference electrode, and the 3D-HPCF or control samples as the working electrodes (WEs) with 6 M KOH as the electrolyte.

RESULTS AND DISCUSSION

The fabrication of 3D-HPCFs is demonstrated in Scheme 1. First, the commercial sponge with a 3D-interconnected macroporous framework was coated with GOCs by a simple "dipping and drying" process in a GOC ink suspension. Next, the resulting GOCs-sponge (GOCSs) was used as a substrate for surface self-assembly of Pluronic F127 templates, PF, and tetraethoxysilane (TEOS) precursors. After carbonization and subsequent HF etching, the sponge and F127 surfactant were removed, the PF was transferred to amorphous carbon, the silicates were removed by HF, the GO was reduced to graphene (reduced graphene oxide), and finally the 3D-HPCFs can be successfully constructed.

The morphology and microstructure of the as-prepared 3D-HPCFs were first characterized by scanning electron microscopy (SEM) and transmission electron microscopy (TEM). Figure 1a shows the typical 3D interconnected macrostructures of the GOCSs with randomly opened

Scheme 1. Fabrication of 3D-HPCFs[a]

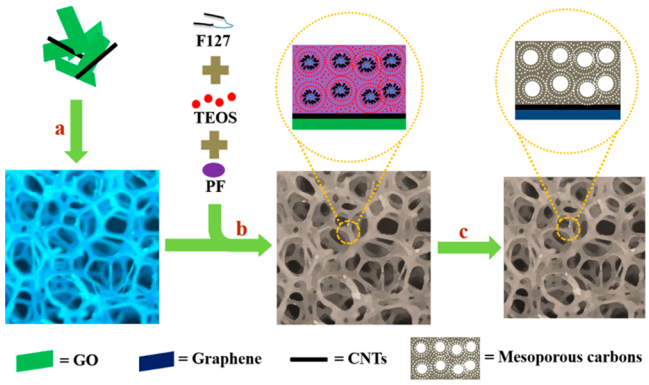

[a](a) Impregnating sponge into the GOCs solution. (b) Impregnating the resulting GOCSs into the multicomponent ethanol solution of F127, PF, and TESO for self-assembly. (c) Carbonization and subsequent etching removal of SiO_2 from TEOS.

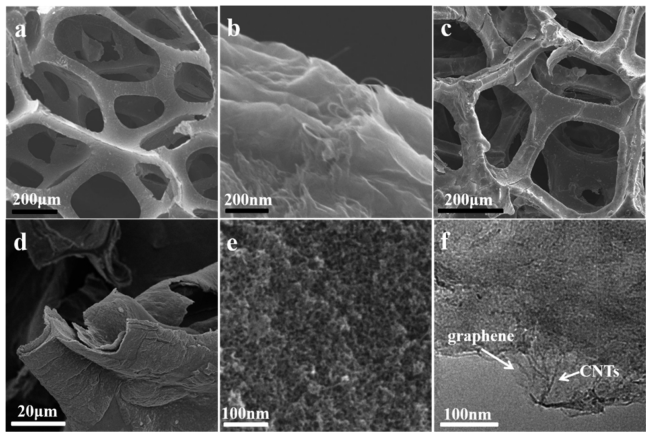

Figure 1. SEM images of (a, b) GOCSs and (c–e) 3D-HPCFs. (f) TEM image of 3D-HPCFs. Additional images are given in Figure S2b–d (Supporting Information).

macropores templated from the framework of PU foams, which is similar to the original sponge (Figure S2a, Supporting Information). The close-up SEM image (Figure 1b) confirms the numerous cracks of GOCs because of the inserted pristine CNTs and their uniform coating onto the sponge due to the strong van der Waals interaction with sponge microfibers.[17] As proved by our previously reports,[6,8] the inserted CNTs not only prevent the aggregation of graphene but also improve the whole conductivity of the composites, which are conducive for SCs or other energy storage applications.

The changes of color and Raman spectra for the sponge also validate the conformal coating of GOCs (Figure S3, Supporting Information). After surface self-assembly, carbonization under Ar, and subsequent HF etching, the resulting 3D-HPCFs inherit the 3D interconnected macrostructures of GOCSs (Figure 1c), with only shrinkage due to the high-temperature carbonization (Figure S3c) even if the sponges are removed (as evidenced by TGA analysis, Figure S4, Supporting Information). The graphene/CNTs are not visible in the high-magnification SEM image (Figure 1d), suggesting that they were completely coated by the bimodal mesoporous carbons. High-resolution SEM (HR-SEM) image (Figure 1e) reveals that the resulting 3D-HPCFs possess mesopores with a diameter of about 5 nm. Remarkably, the TEM image (Figure 1f; for more images, see Figure S2b–d, Supporting Information) clearly shows that the graphene and CNTs (GCs) are well-dispersed in the mesoporous carbon networks. The size of mesopores is about 5 nm, which is consistent with the HR-SEM results (Figure 1e).

To further confirm the porosity feature of 3D-HPCFs, nitrogen adsorption–desorption measurements were employed. Figure 2a shows a type-IV isotherm with a sharp

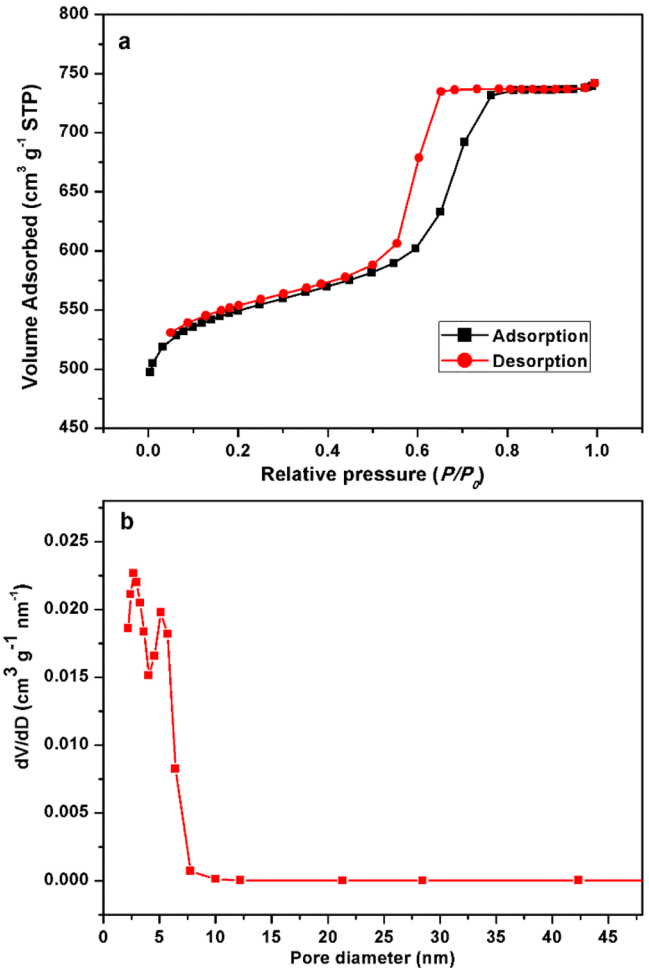

Figure 2. (a) N_2 sorption isotherms and (b) pore size distribution curve of 3D-HPCFs.

capillary condensation step in the relative pressure (P/P_0) range from 0.4 to 0.8 and an obvious H_2-type hysteresis loop, implying the presence of relatively large macropores and mesopores in the frameworks.[16,18,19] Distinct sorption in the isotherm curves at a P/P_0 of 0.1–0.3 is observed, suggesting the presence of smaller pores with a wide distribution below 3.5 nm. The pore size distribution curve calculated from the adsorption branch of the isotherm exhibits bimodal pores with sizes of 5.1 and 2.7 nm due to the decomposition of F127 and removal of silicas from TEOS, respectively.[18] On the basis of the standard Brunauer–Emmett–Teller (BET) method, the specific surface area of 3D-HPCFs is 1286 m^2 g^{-1}, which is significantly higher than that of the other carbon-based porous materials and slightly lower than that of the laser scribed graphene (Table S1, Supporting Information).[4,16,19,20]

Taking into account the unique porous feature of the 3D-HPCFs, we then evaluated their electrochemical performance

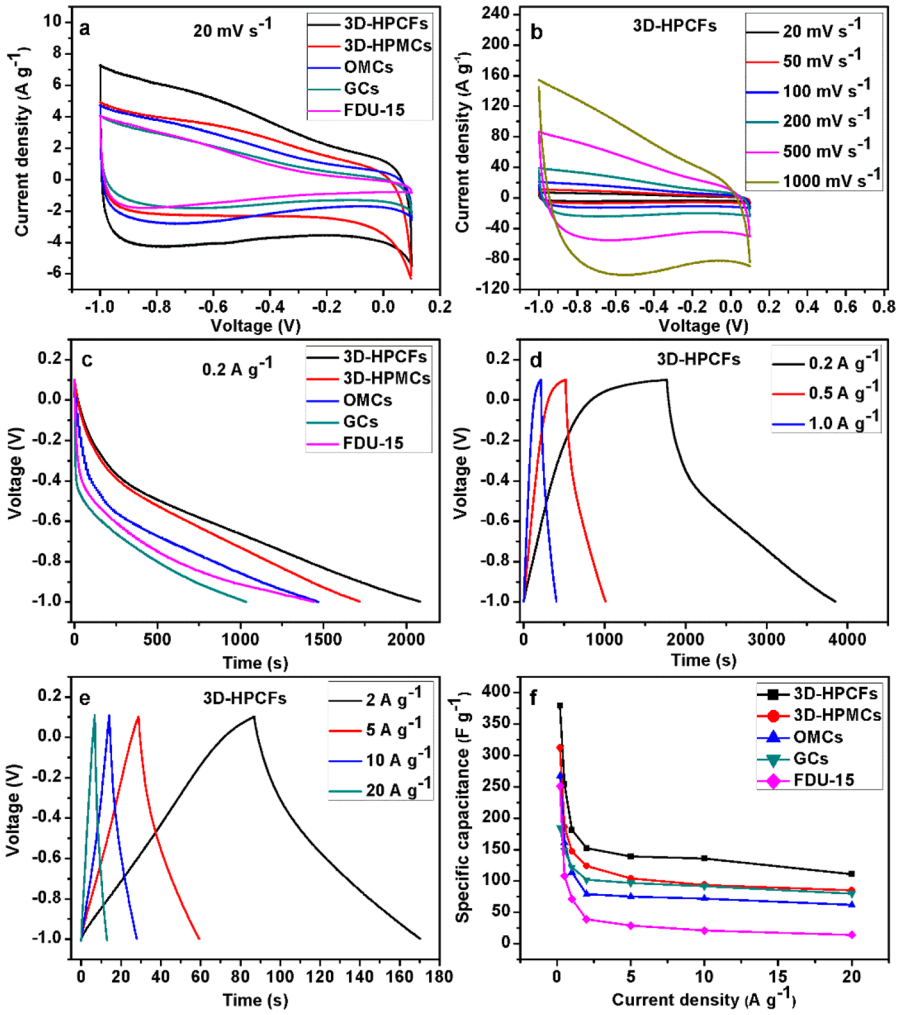

Figure 3. Cyclic voltammetry of (a) all the samples at a scan rate of 20 mV s^{-1} and (b) 3D-HPCFs at different scan rates. The galvanostatic charge−discharge curves of (c) all the samples at a current density of 0.2 A g^{-1} and (d, e) 3D-HPCFs at different current densities. (f) The variation of specific capacitances with current densities for all the samples.

as electrodes for SCs, applying 6 M KOH as electrolyte. As shown in Figure 3a, the cyclic voltammetry profiles (CVs) for 3D-HPCFs electrodes exhibit more rectangular shapes and higher current density at the scan rate of 20 mV s^{-1} than the other samples, representing more ideal capacitive behavior, lower resistance, and higher capacitance. Typically, the CVs of the 3D-HPCFs electrode still retain the relatively rectangle shape even though the scan rate increased from 20 to 1000 mV s^{-1} (Figure 3b), indicating a typical electrical double-layer behavior and the superior ion response.[12] The applicability of supercapacitors can be directly evaluated by means of the galvanostatic charge−discharge method. Plots of voltage versus time for all the samples at different current densities are displayed in Figure 3c and Figure S5 (Supporting Information). The galvanostatic (GV) discharge time of the 3D-HPCFs electrode is significantly greater than that of the control samples at the same current density, implying its larger charge capacity, which is coincident with the CV results. In addition, the typical triangular profiles also confirm its good electrochemical capacitive property (Figure 3d,e). The specific capacitances derived from the discharging curves (for details, see the Supporting Information) at different current densities, as summarized in Figure 3f, clearly indicate that 3D-HPCFs result in a greatly improved capacitance. For instance, the specific capacitance obtained at 0.2 A g^{-1} for 3D-HPCFs is 379 F g^{-1}, which is much higher than that of 3D hierarchically mesoporous carbons (3D-HPMCs, 312 F g^{-1}) without GCs (Figure S6a,b, Supporting Information); bimodal ordered mesoporous carbon monoliths (OMCs, 267 F g^{-1}) without 3D macropores and GCs (Figure S6c,d); FDU-15 mesoporous carbons (251 F g^{-1}) without GCs, 3D macropores, and complementary pores (Figure S6g,h); GCs (185 F g^{-1}, Figure S6e,f); and other nanocarbon-based materials (Table S2, Supporting Information). These parallel experiments strongly suggest the critical importance of hierarchically porous frameworks and conductivity to improve the electrochemical performance: (1) the 3D interconnected macrostructures can buffer electrolytes to reduce ion transport resistance and minimize ion diffusion distance to the interior surfaces of the mesopores; (2) the bimodal mesopores, together with numerous cracks of GCs due to the inserted pristine CNTs, can enhance charge storage and ion transport; and (3) the conductive GCs within 3D networks can synergistically facilitate the electron transfer in the bulk electrode. Furthermore, the 3D-HPCFs electrode displays good capacitance retention (Figure 3f). For example, the highest specific capacitance of ∼111 F g^{-1} was obtained among our measured samples at a high current density of 20 A g^{-1}, demonstrating

the reduced ion transport limitation in 3D hierarchically porous materials, the highly accessible surface areas, and increased electrical conductivity.[16] Moreover, the volumetric capacities for 3D-HPCFs are 344.5, 230.9, 164.5, 138.2, 126.4, 123.7, and 100.9 F cm^{-3} at current densities of 0.2, 0.5, 1.0, 2.0, 5.0, 10, and 20 F g^{-1}, respectively, which are higher than that of self-assembled block copolymer-derived nitrogen-enriched nanocarbons with a specific surface area of 500 m^2 g^{-1} (wherein, the volumetric capacity is 185.1 F cm^{-3} at 0.1 A g^{-1}), the CO_2-activated benchmark with a specific surface area of 1140 m^2 g^{-1} (wherein, the volumetric capacity is 138.5 F cm^{-3} at 0.1 A g^{-1}), and the KOH-activated benchmark with a specific surface area of 2570 m^2 g^{-1} (wherein, the volumetric capacity is 81.2 F cm^{-3} at 0.1 A g^{-1}).[21] It should be noted that the volumetric energy density of 3D-HPCFs is not very high, which is common for the nanoarchitecture with a high specific surface area. Further efforts regarding the improvement of volumetric energy density should be made. Also, we compared the energy densities of the 3D-HPCFs and the control samples at various current densities and maximum power densities, as shown in Figure S7 (Supporting Information). The energy and power densities were calculated by means of constant-current charging–discharging of a supercapacitor electrode using a cell-voltage window of 1.1 V and current densities between 0.2 and 20 A g^{-1} (see the Supporting Information for details). The energy density of 3D-HPCFs decreases from 63.7 to 18.7 Wh kg^{-1}, whereas the power density increases from 0.1 to 11.0 kW kg^{-1}. These values are higher than those of the other four samples.

Another important requirement for supercapacitor application is cycling lifetime. Tests over 2000 cycles for the 3D-HPCFs sample at current densities of 5 and 10 A g^{-1} were carried out by using the galvanostatic charge–discharge cycling techniques; the results are shown in Figure 4. The 3D-HPCFs

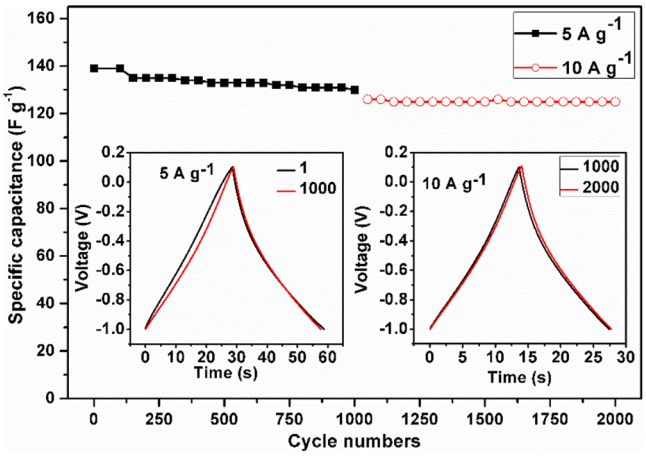

Figure 4. Specific capacitance of 3D-HPCFs electrode for a 2000-cycle charge–discharge test at current densities of 5 and 10 A g^{-1}. The inset shows the galvanostatic charge–discharge curves of 3D-HPCFs electrode at current densities of 5 A g^{-1} at the 1st and 1000th (left) and 10 A g^{-1} at the 1000th and 2000th (right).

electrode exhibits excellent performance stability with 94% retention in capacitance (130 F g^{-1}, Figure S8, Supporting Information) after 1000 charge–discharge cycles at a current density of 5 A g^{-1}. The charge–discharge profiles after 1000 cycles retain linearity and symmetry well as the first cycle (Figure 4, inset, left). When the current density is further increased to 10 A g^{-1}, the 3D-HPCFs electrode still shows 99% retention in capacitance (125 F g^{-1}, Figure 4 and Figure S9, Supporting Information) and the shape of charge–discharge curves hardly changes (Figure 4, inset, right) after another 1000 cycles. The pronounced mechanical stability may be attributed to the presence of GCs as well as their positive effect on the porous carbon material contacts and the mechanical integrity of the composite active mass upon prolonged cycling.

To gain insight into the supercapacitor behavior of 3D-HPCFs, electrochemical impedance spectroscopy (EIS) was performed in the frequency range from 0.1 Hz to 100 kHz with a bias potential of 0 V vs saturated calomel electrode (SCE). The Nyquist plots for 3D-HPCFs are shown in Figure 5,

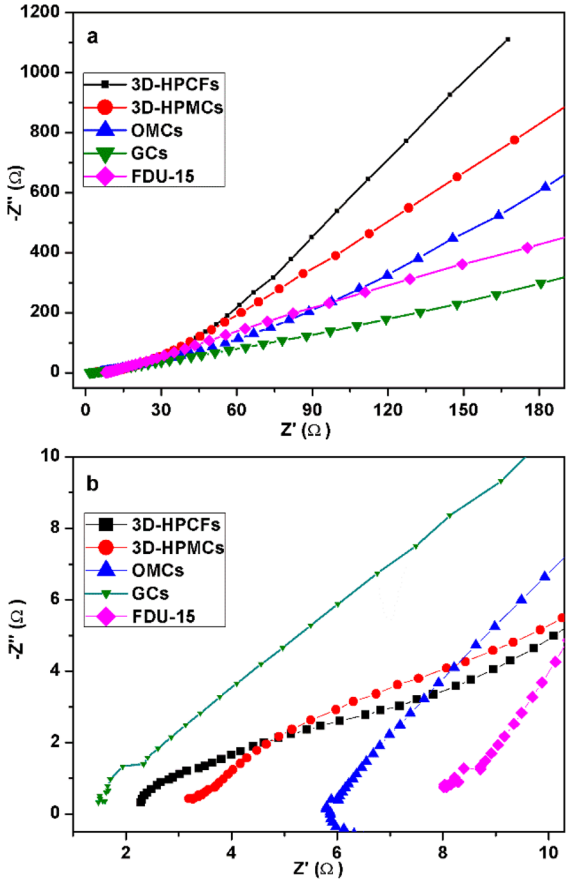

Figure 5. (a) Nyquist plots and (b) the expanded Nyquist plots at high frequency for all the samples.

together with other control samples of 3D-HPMCs, OMCs, GCs, and FDU-15. All of the Nyquist plots show a straight line in the low frequency region and an arc in the high frequency region. At high frequency (close to 100 kHz), the intercept with the Z' axis (real impedance axis) represents the intrinsic Ohmic resistance of the internal resistance or equivalent series resistance (ESR) of the electrode material and electrolyte.[22] As shown in Figure 5b, the expanded view, 3D-HPCFs electrode shows a quite low value (2.2 Ω), which is much lower than the control materials (3.2, 5.8, and 8.0 Ω for 3D-HPMCs, OMCs, and FDU-15, respectively) and slightly higher than the GCs (1.6 Ω). These results clearly demonstrate that incorporating highly conductive GCs effectively reduces electrical resistance. At low frequency, the slope of the linear plots reflects the diffusive resistivity of the electrolyte ions within the pores (Figure 5a). A steeper gradient corresponds to faster ion

dx.doi.org/10.1021/am503783t | ACS Appl. Mater. Interfaces 2014, 6, 15302–15308

diffusion and, therefore, is more representative of an ideal capacitor.[9,23−26] Clearly, the slope for 3D-HPCFs is larger than that of other samples, suggesting faster ion diffusion and more ideal capacitive behavior. This is because the 3D interconnected macrostructures could buffer electrolytes to reduce ion transport resistance and minimize ion diffusion distance and the bimodal mesopores together with numerous cracks of GCs due to the inserted pristine CNTs also enhance charge storage and ion transport.[27−29]

CONCLUSION

We have successfully synthesized new 3D hierarchically porous carbon-CNT-graphene ternary all-carbon foams (3D-HPCFs) though multicomponent surface self-assembly of graphene oxide-dispersed CNTs (GOCs) supported on a commercial sponge. The sponge with an interconnected macroporous framework serves as a 3D scaffold for supporting GOCs and subsequently multicomponent self-assembly; the GO acts as "surfactant" to directly disperse pristine CNTs, preserving the excellent electronic structure of pristine CNTs and preventing the aggregation of graphene (reduced from GO) as well as improving the whole conductivity. As a result, the resulting 3D-HPCFs possess 3D macro- and mesoporous structures, a high specific surface area (1286 m^2 g^{-1}), large bimodal mesopores (5.1 and 2.7 nm), and excellent high conductivity, and then the 3D-HPCFs-based supercapacitors show outstanding specific capacitance, high rate capability, and excellent cycling stability, making them very promising for the next-generation advanced energy storage devices. Moreover, we believe that the excellent characteristics are even more compelling for other applications, such as adsorbents, catalyst supports, photovoltaic cells, and lithium-ion batteries. Further studies along this line are in progress.

ASSOCIATED CONTENT

Supporting Information

The digital photographs of GO, CNTs, GOCs, commercially available sponge, GO-dispersed pristine CNTs (GOCs) supported on sponge (GOCSs), and 3D hierarchically porous all-carbon foams; SEM images and TEM images of the control samples; Raman spectra of GOCSs; TGA and DTG curves of commercially available sponge and triblock copolymer Pluronic F127 in Ar flow; galvanostatic discharge curves at various discharge current densities; and the comparison of specific surface area and specific capacitance. This material is available free of charge via the Internet at http://pubs.acs.org.

AUTHOR INFORMATION

Corresponding Author

*E-mail: youbo@mail.ustc.edu.cn (B.Y.).

Notes

The authors declare no competing financial interest.

ACKNOWLEDGMENTS

We acknowledge Prof. Z. X. Deng and J. Yang for experimental support.

REFERENCES

(1) Simon, P.; Gogotsi, Y. Materials for Electrochemical Capacitor. *Nat. Mater.* **2008**, *7*, 845−854.

(2) Li, W.; Wang, F.; Feng, S. S.; Wang, J. X.; Sun, Z. K.; Li, B.; Li, Y. H.; Yang, J. P.; Elzatahry, A. A.; Xiao, Y. Y.; Zhao, D. Y. Sol-Gel Design Strategy for Ultradispersed TiO_2 Nanoparticles on Graphene for High-Performance Lithium Ion Batteries. *J. Am. Chem. Soc.* **2014**, *136*, 18300−18303.

(3) EI-Kady, M. F.; Strong, V.; Dubin, S.; Kaner, R. B. Laser Scribing of High-Performance and Flexible Graphene-Based Electrochemical Capacitors. *Science* **2012**, *335*, 1326−1330.

(4) Li, W.; Zhang, F.; Dou, Y. Q.; Wu, Z. X.; Liu, H. J.; Qian, X. F.; Gu, D.; Xia, Y. Y.; Tu, B.; Zhao, D. Y. A Self-Template Strategy for the Synthesis of Mesoporous Carbon Nanofibers as Advanced Supercapacitor Electrodes. *Adv. Energy Mater.* **2011**, *1*, 382−386.

(5) Wang, H. L.; Xu, Z. W.; Kohandehghan, A.; Li, Z.; Tan, X. B.; Stephenson, T. J.; King'ondu, C. K.; Holt, C. M. B.; Olsen, B. C.; Tak, J. K.; Harfield, D.; Anyia, A. O.; Mitlin, D. Interconnected Carbon Nanosheets Derived from Hemp for Ultrafast Supercapacitors with High Energy. *ACS Nano* **2013**, *7*, 11004−11015.

(6) You, B.; Li, N.; Zhu, H. Y.; Zhu, X. L.; Yang, J. Graphene Oxide-Dispersed Pristine CNTs Support for MnO_2 Nanorods as High Performance Supercapacitor Electrodes. *ChemSusChem* **2013**, *6*, 474−480.

(7) You, B.; Wang, L. L.; Li, N.; Zheng, C. L. Improving the Energy Storage Performance of Graphene through Insertion of Pristine CNTs and Ordered Mesoporous Carbon Coating. *ChemElectroChem* **2014**, *1*, 772−778.

(8) You, B.; Wang, L. L.; Yao, L.; Yang, J. Three Dimensional N-Doped Graphene-CNT Networks for Supercapacitor. *Chem. Commun.* **2013**, *49*, 5016−5018.

(9) Wang, X. F.; Raju, V.; Luo, W.; Wang, B.; Stickle, W. F.; Ji, X. L. Ambient Hydrolysis Deposition of TiO_2 in Nanoporous Carbon and the Converted TiN-Carbon Capacitive Electrode. *J. Mater. Chem. A* **2014**, *2*, 2901−2905.

(10) Noked, M.; Okashy, S.; Zimrin, T.; Aurbach, D. Composite Carbon Nanotube/Carbon Electrodes for Electrical Double-Layer Supercapacitors. *Angew. Chem., Int. Ed.* **2012**, *51*, 1568−1571.

(11) Meng, Y.; Gu, D.; Zhang, F. Q.; Shi, Y. F.; Yang, H. F.; Li, Z.; Yu, C. Z.; Tu, B.; Zhao, D. Y. Ordered Mesoporous Polymers and Homologous Carbon Frameworks: Amphiphilic Surfactant Templating and Direct Transformation. *Angew. Chem., Int. Ed.* **2005**, *44*, 7053−7059.

(12) Wang, D. W.; Li, F.; Liu, M.; Lu, G. Q.; Cheng, H. M. 3D Aperiodic Hierarchical Porous Graphitic Carbon Material for High-Rate Electrochemical Capacitive Energy Storage. *Angew. Chem., Int. Ed.* **2008**, *47*, 373−376.

(13) Zhang, L.; Yang, X.; Zhang, F.; Long, G. K.; Zhang, T. F.; Leng, K.; Zhang, Y. W.; Huang, Y.; Ma, Y. F.; Zhang, M. T.; Cheng, Y. S. Controlling the Effective Surface Area and Pore Size Distribution of sp^2 Carbon Materials and Their Impact on the Capacitance Performance of These Materials. *J. Am. Chem. Soc.* **2013**, *135*, 5921−5929.

(14) Chen, W.; Rakhi, R. B.; Hu, L. B.; Xie, Y.; Cui, Y.; Alshareef, H. N. High-Performance Nanostructured Supercapacitor Sponge. *Nano Letter.* **2011**, *11*, 5165−5172.

(15) Yang, S. B.; Feng, X. L.; Wang, L.; Tang, K.; Maier, J.; Müllen, K. Graphene-Based Nanosheets with a Sandwich Structure. *Angew. Chem., Int. Ed.* **2010**, *49*, 4795−4799.

(16) Wu, Z. S.; Sun, Y.; Tan, Y. Z.; Yang, S. B.; Feng, X. L.; Müllen, K. Three-Dimensional Graphene-Based Macro- and Mesoporous Frameworks for High-Performance Electrochemical Capacitive Energy Storage. *J. Am. Chem. Soc.* **2012**, *134*, 19532−19535.

(17) Ge, J.; Yao, H. B.; Wang, X.; Ye, Y. D.; Wang, J. L.; Wu, Z. Y.; Liu, J. W.; Fan, F. J.; Gao, H. L.; Zhang, C. L.; Yu, S. H. Stretchable Conductors Based on Silver Nanowires: Improved Performance through a Binary Network Design. *Angew. Chem., Int. Ed.* **2012**, *52*, 1654−1659.

(18) You, B.; Yang, J.; Sun, Y. Q.; Su, Q. D. Easy Synthesis of Hollow Core, Bimodal Mesoporous Shell Carbon Nanospheres and Their Application in Supercapacitor. *Chem. Commun.* **2011**, *47*, 12364−12366.

(19) Fang, Y.; Lv, Y. Y.; Che, R. C.; Wu, H. Y.; Zhang, X. H.; Gu, D.; Zheng, F.; Zhao, D. Y. Two-Dimensional Mesoporous Carbon

Nanosheets and Their Derived Graphene Nanosheets: Synthesis and Efficient Lithium Ion Storage. *J. Am. Chem. Soc.* **2013**, *135*, 1524−1530.
(20) Fan, Z. J.; Yan, J.; Zhi, L. J.; Zhang, Q.; Wei, T.; Feng, J.; Zhang, M. L.; Qian, W. Z.; Wei, F. A Three-Dimensional Carbon Nanotube/Graphene Sandwich and Its Application as Electrode in Supercapacitors. *Adv. Mater.* **2010**, *22*, 3723−3728.
(21) Zhong, M. J.; Kim, E. K.; McGann, J. P.; Chun, S. E.; Whitacre, J. F.; Jaroniec, M.; Matyjaszewski, K.; Kowalewski, T. Electrochemically Active Nitrogen-Enriched Nanocarbons with Well-Defined Morphology Synthesized by Pyrolysis of Self-Assembled Block Copolymer. *J. Am. Chem. Soc.* **2012**, *134*, 14846−14857.
(22) Choi, B. G.; Hong, J.; Hong, W. H.; Hammond, P. T.; Park, H. Facilitated Ion Transport in All-Solid-State Flexible Supercapacitors. *ACS Nano* **2011**, *5*, 7205−7213.
(23) Largeot, C.; Portet, C.; Chmiola, J.; Taberna, P.; Gogotsi, Y.; Simon, P. Relation between the Ion Size and Pore Size for an Electric Double-Layer Capacitor. *J. Am. Chem. Soc.* **2008**, *130*, 2730−2731.
(24) Lee, G.; Cheng, Y. W.; Varanasi, C. V.; Liu, J. Influence of the Nickel Oxide Nanostructure Morphology on the Effectiveness of Reduced Graphene Oxide Coating in Supercapacitor Electrodes. *J. Phys. Chem. C* **2014**, *118*, 2281−2286.
(25) Coadou, E.; Timperman, L.; Jacquemin, J.; Galiano, H.; Hardacre, C.; Anouti, M. Comparative Study on Performances of Trimethyl-Sulfonium and Trimethyl-Ammonium Based Ionic Liquids in Molecular Solvents as Electrolyte for Electrochemical Double Layer Capacitors. *J. Phys. Chem. C* **2013**, *117*, 10315−10325.
(26) Li, W.; Zhao, D. Y. An Overview of the Synthesis of Ordered Mesoporous Materials. *Chem. Commun.* **2013**, *49*, 943−946.
(27) Falco, C.; Sieben, J. M.; Brun, N.; Sevilla, M.; Mauelen, T.; Morallon, E.; Cazorla-Amoros, D.; Titirici, M. M. Hydrothermal Carbons from Hemicellulose-Derived Aqueous Hydrolysis Products as Electrode Materials for Supercapacitors. *ChemSusChem* **2013**, *6*, 374−382.
(28) Zhang, D.; Dong, Q. Q.; Wang, X.; Yan, W.; Deng, W.; Shi, L. Y. Preparation of a Three-Dimensional Ordered Macroporous Carbon Nanotube/Polypyrrole Composite for Supercapacitors and Diffusion Modeling. *J. Phys. Chem. C* **2013**, *117*, 20446−20455.
(29) Lee, J. S.; Kim, S. I.; Yoon, J. C.; Jang, J. H. Chemical Vapor Deposition of Mesoporous Graphene Nanoballs for Supercapacitor. *ACS Nano* **2013**, *7*, 6047−6055.